The *Caenorhabditis elegans odr-2* Gene Encodes a Novel Ly-6-Related Protein Required for Olfaction

Joseph H. Chou, Cornelia I. Bargmann and Piali Sengupta[1]

Howard Hughes Medical Institute, Programs in Developmental Biology, Neuroscience, and Genetics, Department of Anatomy and Department of Biochemistry and Biophysics, University of California, San Francisco, California 94143-0452

Manuscript received August 14, 2000
Accepted for publication October 5, 2000

ABSTRACT

Caenorhabditis elegans odr-2 mutants are defective in the ability to chemotax to odorants that are recognized by the two AWC olfactory neurons. Like many other olfactory mutants, they retain responses to high concentrations of AWC-sensed odors; we show here that these residual responses are caused by the ability of other olfactory neurons (the AWA neurons) to be recruited at high odor concentrations. *odr-2* encodes a membrane-associated protein related to the Ly-6 superfamily of GPI-linked signaling proteins and is the founding member of a *C. elegans* gene family with at least seven other members. Alternative splicing of *odr-2* yields three predicted proteins that differ only at the extreme amino terminus. The three isoforms have different promoters, and one isoform may have a unique role in olfaction. An epitope-tagged ODR-2 protein is expressed at high levels in sensory neurons, motor neurons, and interneurons and is enriched in axons. The AWC neurons are superficially normal in their development and structure in *odr-2* mutants, but their function is impaired. Our results suggest that ODR-2 may regulate AWC signaling within the neuronal network required for chemotaxis.

CAENORHABDITIS elegans is an excellent model system for the study of behavior because of its simple nervous system and genetic tractability (Brenner 1974). A complete wiring diagram of its nervous system has been elucidated by serial section electron microscopy, identifying the circuits that generate behavior (White *et al.* 1986). The contribution of specific neurons to various behaviors can be assessed by using a laser microbeam to ablate individual neurons, while the molecules required can be revealed by genetic analysis (Bargmann 1993). *C. elegans* senses volatile attractants using two pairs of olfactory neurons, AWA and AWC (Bargmann *et al.* 1993). The AWA and AWC neurons each detect several attractive volatile odorants. Genetic screens for mutants unable to chemotax to odorants have identified molecules required for olfactory behaviors. A number of olfactory signaling components have been identified in these screens, including odorant receptors, G proteins, and ion channels, as well as proteins important for receptor localization to the sensory cilia and transcription factors that determine the functional identity of chemosensory neurons (Sengupta *et al.* 1994, 1996; Coburn and Bargmann 1996; Komatsu *et al.* 1996; Colbert *et al.* 1997; Dwyer *et al.* 1998; Roayaie *et al.* 1998; Sagasti *et al.* 1999). These studies have defined a framework for the initial events of olfactory perception and signaling. However, several aspects of *C. elegans* olfaction remain poorly understood. First, the defects in the olfactory mutants are most striking in a limited range of odor concentrations (Bargmann *et al.* 1993). It is not known whether this concentration dependence is due to residual gene activity in the mutants, parallel functions in multiple olfactory neurons, or nonspecific odor-sensing pathways. Second, the mechanisms by which olfactory neurons interact with interneurons and regulatory circuits to generate chemotactic behavior are not understood.

Ly-6 proteins were originally defined as murine lymphocyte cell surface differentiation antigens (LeClair *et al.* 1986; Gumley *et al.* 1995). They are a superfamily of related proteins with sequence similarity in a domain of ~75 amino acids, defined by 10 conserved cysteine residues with a characteristic spacing pattern (Palfree 1996). The Ly-6 domains of all members are extracellular and most are linked to the plasma membrane via a glycosylphosphatidylinositol (GPI) moiety (Low 1989) that is important for their function (Su *et al.* 1991). Ly-6 proteins are also similar to a family of secreted snake neurotoxins with 8 conserved cysteines; the crystal structure of cobratoxin and a solution structure of the Ly-6 protein CD59 demonstrated disulfide bridge pair conservation and overall structural similarity between these two proteins (Betzel *et al.* 1991; Fletcher *et al.* 1994; Kieffer *et al.* 1994).

Here we describe the characterization and cloning of *odr-2*, a novel neuronally expressed gene required for AWC-mediated olfactory behaviors in *C. elegans*. All

Corresponding author: Cornelia Bargmann, Department of Anatomy, University of California, San Francisco, CA 94143-0452.
E-mail: cori@itsa.ucsf.edu

[1]*Present address:* Department of Biology and Volen Center for Complex Systems, Brandeis University, Waltham, MA 02454.

three alleles of *odr-2* are defective in chemotaxis to odorants sensed by AWC, including benzaldehyde, isoamyl alcohol, and low concentrations of 2,3-pentanedione (Bargmann *et al.* 1993; this work). Chemotaxis to odorants sensed by the AWA olfactory neurons is not affected in *odr-2* mutants. Using laser ablations and double mutants, we find that the response to high concentrations of two odors, diacetyl and 2,3-pentanedione, is mediated by parallel functions of the AWA and AWC neurons. This observation helps explain the responses to high concentrations of odors observed in *odr-2* and other olfactory mutants. *odr-2* encodes a predicted membrane-associated protein distantly related to the Ly-6 superfamily that includes a conserved cysteine motif and potential GPI-targeting sequences. Alternative splicing yields different protein isoforms that differ only at the extreme amino terminus. ODR-2 is widely expressed exclusively in neurons, and individual isoforms may be expressed in different sets of neurons. ODR-2 is enriched in axons, and may modulate AWC-specific signaling in the neural circuit required for chemotaxis.

MATERIALS AND METHODS

Strains and genetics: Wild-type worms were *C. elegans* variety Bristol, strain N2. Worms were grown at 20° with abundant food using standard methods (Brenner 1974).

Strains used in this work included CX2304 *odr-2(n2145)* V; CX2058 *odr-2(n1939)* V; MT5304 *odr-2(n2148)* V; CX2818 *lin-15(n765ts)* X; CX2188 *odr-2(n2145)* V; *lin-15(n765ts)* X; CX2065 *odr-1(n1936)* X; CX4 *odr-7(ky4)* X; CX 2335 and CX2336 *odr-7(ky4) odr-1(n1936)* X (two independent isolates); CX2291 and CX2292 *odr-2(n2145)* V; *odr-1(n1936)* X (two independent isolates); CX2337 *odr-2(n2145)* V; and *odr-7(ky4)* X. Double mutants without any additional markers were generated by eliminating linked markers *in trans* to the mutation of interest and were confirmed by complementation tests.

Behavioral assays: All behavioral assays were conducted on well-fed adults. Standard population chemotaxis assays were performed as previously described (Bargmann *et al.* 1993). Briefly, 75–150 washed animals were placed in the center of an agar plate with an odorant diluted in ethanol at one side and an ethanol control at the opposite side. Animals that reached the odorant or control were trapped by a spot of sodium azide. After 1 hr, a chemotaxis index was calculated as [(no. of animals at odorant) − (no. of animals at ethanol)]/[total no. of animals in assay]. A chemotaxis index of 1.0 represents perfect attraction to the odorant, −1.0 represents perfect repulsion, and 0 represents a neutral response. Assay plates were used 1–3 days after pouring.

All alleles of *odr-2* exhibited variability in chemotaxis toward AWC-sensed odorants, but in dose-response assays *odr-2* animals consistently underperformed wild-type animals when challenged with odorants sensed by AWC. Because the threshold of odorant concentrations that distinguished wild-type and *odr-2* animals varied, several different odorants and odorant concentrations were used to follow the *odr-2* phenotype in this work. Unless otherwise noted, the assays shown in each figure used identical odorant concentrations, were conducted during a similar time period, and included simultaneous positive wild-type and negative *odr-2* mutant controls. Statistical analyses were conducted on sets of assays with those characteristics.

Laser killing of the AWA and AWC neurons was performed in L1 larvae using standard methods (Bargmann and Avery 1995). Laser-operated and control animals were tested in single-animal chemotaxis assays as described (Bargmann *et al.* 1993). The single-animal assay is scored by examining the tracks an animal leaves on a plate with a single spot of odorant. The baseline (false-positive) rate for this assay is 0.11; values greater than this indicate a response to the odorant, with 1.0 representing a perfect chemotaxis response.

Molecular biology methods: General manipulations were performed using standard methods (Sambrook *et al.* 1989). Sequencing was performed with the Promega (Madison, WI) *fmol* sequencing kit in an MJR thermal cycler. The GeneWorks v2.5.1 software package (IntelliGenetics, Mountain View, CA) and DNA Strider v1.2 (public domain, by Christian Marck) was used for sequence analysis. BLAST (Altschul *et al.* 1990) and CLUSTALW (Thompson *et al.* 1994) were both used to generate sequence alignments; however, manual alignment of cysteine residues was frequently done prior to software-assisted alignment. Sequence of the *odr-2* genomic region was generated in the lab and confirmed with data courtesy of the *C. elegans* Sequencing Consortium (1998; Sulston *et al.* 1992).

Generation of transgenic worms: Transgenic strains were generated by standard microinjection methods (Mello *et al.* 1991). All injections were done in lines bearing the *lin-15(n765ts)* mutation. Unless otherwise noted, test DNA was injected at 50 ng/μl with wild-type *lin-15* DNA pJM23 (50 ng/μl) as a co-injection marker. Rescued lines were isolated from independent rescued F_1 progeny.

Generation of hemagglutinin epitope-tagged *odr-2* clones: PCR-directed insertional mutagenesis was used to insert the hemagglutinin (HA) epitope tag in five different locations of the 1.9-kb *Kpn*I-*Xho*I genomic fragment that contains the entire *odr-2* common region. Each fragment was inserted in-frame at the sites shown in Figure 2D and consisted of 5′-GCC TAC CCA TAT GAT GTC CCA GAC TAC GCT GGA TCC-3′, which codes for the amino acids Ala [Tyr Pro Tyr Asp Val Pro Asp Tyr Ala] Gly Ser; the bracketed residues represent the HA epitope. Note that the last six nucleotides insert a *Bam*HI restriction site. Oligonucleotide JHC-27, which is 5′ to the *Xho*I site, and JHC-28, which is 3′ to the *Kpn*I site, were used for all epitope insertions. A 5′ fragment was generated by PCR amplification using JHC-27 and a "JHC-##b" oligo, while a partially overlapping 3′ fragment was generated using JHC-28 and a "JHC-##a" oligo. These two fragments were gel purified and used as template to amplify the complete epitope-tagged *Kpn*I-*Xho*I fragment using JHC-27 and JHC-28. The five PCR-derived *Kpn*I-*Xho*I fragments containing the epitope insertions were used to replace the corresponding wild-type region in a rescuing *Kpn*I-*Spe*I clone in pBluescript II KS(−).

5′ oligo: JHC-27: 5′-TTT ACG TAT CGA CAA TTG CGC GCA G-3′

3′ oligo: JHC-28: 5′-CTA CTT ACT GTT CAG GAA GGT TAT G-3′

HA#1: (JHC-29a) 5′-CCA TAT GAT GTC CCA GAC TAC GCT GGA TCC CGT CTA CCA TGT TAC TCC TG-3′
(JHC-29b) 5′-AGC GTA GTC TGG GAC ATC ATA TGG GTA GGC TAG TGC TGA AAA AAT AAT AT-3′

HA#2: (JHC-30a) 5′-CCA TAT GAT GTC CCA GAC TAC GCT GGA TCC TTC GAC ACT CAT TGC GAT AA-3′
(JHC-30b) 5′-AGC GTA GTC TGG GAC ATC ATA TGG GTA GGC AGA AAG TGG TTT CCG GTA CA-3′

HA#3: (JHC-31a) 5′-CCA TAT GAT GTC CCA GAC TAC GCT GGA TCC GAT ATG TGT GTT ACT CTT AG-3′
(JHC-31b) 5′-AGC GTA GTC TGG GAC ATC ATA TGG GTA GGC GGA ACA GTT CTT TGA GTA GA-3′

HA#4: (JHC-32a) 5′-CCA TAT GAT GTC CCA GAC TAC GCT GGA TCC CAG GGA TGC TTG GGT GAG TT-3′
(JHC-32b) 5′-AGC GTA GTC TGG GAC ATC ATA TGG GTA GGC CCT TTC AGC CAA CGT TCG AA-3′
HA#5: (JHC-33a) 5′-CCA TAT GAT GTC CCA GAC TAC GCT GGA TCC AAT TTC TCC GTG TCG CCG CC-3′
(JHC-33b) 5′-AGC GTA GTC TGG GAC ATC ATA TGG GTA GGC GCA CAG ATT GTT ATG GCA TG-3′

Antibody staining: Glass microscope slides were treated with 0.1% w/v polylysine and allowed to air dry overnight. Worms were washed extensively in S Basal and H_2O, transferred to the coated slides, flattened slightly under a glass coverslip, and allowed to settle for 3 min at room temperature. Following freeze fracture on a slab of dry ice, the worms were fixed 5 min in methanol and 5 min in acetone and blocked for 1 hr at room temperature in PBS + 0.1% BSA + 0.2% Tween-20. The samples were then treated with primary anti-HA epitope monoclonal antibodies (BAbCo mouse monoclonal antibody HA.11, clone 16B12) at a 1:500 dilution into blocking solution for 1 hr at room temperature, washed with PBS + 0.2% Tween-20, incubated with secondary antibodies (Cy3-conjugated AffiniPure goat anti-mouse IgG; Jackson ImmunoResearch Laboratories, West Grove, PA) at a 1:500 dilution in blocking solution, washed in PBS + 0.2% Tween-20, and visualized by fluorescence microscopy.

Generation of *odr-2* green fluorescent protein clones: Regions immediately upstream of the *odr-2* 2b, 16, and 18 isoforms and *hot-1a* predicted initiator methionines were isolated by PCR for use as transcriptional promoter fusions driving green fluorescent protein (GFP). Cosmid EB2 subclones and genomic DNA isolated from wild-type animals were used as templates for *odr-2* and *hot-1a* promoters, respectively. The PCR primers incorporated convenient restriction sites and were designed using sequence provided by the *C. elegans* Genome Sequencing Consortium. GFP vectors were provided by Andy Fire. The *odr-2* 2b promoter (2.6 kb) was isolated as a *Spe*I fragment and cloned into the *Xba*I site of TU#62. *odr-2* 16 (3.2 kb), *odr-2* 18 (2.4 kb), and *hot-1a* (4.1 kb) promoters were isolated as *Pst*I-*Bam*HI fragments and cloned into wild-type GFP vector TU#62, except for the isoform 16 promoter, which was cloned into the pPD95.77 GFP vector. Oligonucleotide sequences are available upon request.

A 10.8-kb *odr-2 Sph*I fragment was cloned in-frame as a translational fusion into the TU#62 GFP vector modified to contain the synthetic transmembrane domain from pPD34.110 (Fire *et al.* 1990).

AWC promoter driving *odr-2* cDNA expression: A 3.7-kb promoter fragment of the *str-2* gene (which drives expression in AWC chemosensory neurons, Troemel *et al.* 1999) was PCR-amplified and cloned upstream of each of the *odr-2* 2b, 16, and 18 cDNAs. The plasmid backbone was the pBlueScript vector used for the original isolation of the cDNAs.

Generation of internal deletions of *odr-2*: Internal deletions were made in the *Kpn*I-*Spe*I and *Kpn*I-*Spe*I HA#3 *odr-2* rescuing constructs. Clones with multiple deletions were made by introducing individual deletions sequentially. The 2b alternative region was deleted by cutting with PmlI and religating; Δ2b deletes a total 159 bp, including both in-frame methionines that could serve to initiate translation. The 16 alternative region was deleted by cutting with *Avr*II and *Afl*II, blunting the ends with Klenow polymerase, and religating; Δ16 deletes 652 bp, including the entire alternative exon, 46 bp before the predicted initiation methionine and 529 bp from the following intron. The 18 alternative region was deleted in the *Kpn*I-*Spe*I HA#3 construct. First, the *Eag*I site in the pBluescript II KS(−) polylinker was destroyed by cutting with *Spe*I and *Not*I, blunting with Klenow polymerase, and religating. The 18 alternative region was then deleted by cutting with *Eag*I and religating; Δ18 deletes 1553 bp, starting 2 bp after the predicted initiator methionine and extending 1494 bp into the following intron. The Δ*Bst*EII subclone was made by cutting with *Bst*EII, blunting with Klenow polymerase, and religating; Δ*Bst*EII deletes 2.6 kb, including the entire isoform 18 alternative exon. Δ*Cla*I was made by cutting with *Cla*I and religating; Δ*Cla*I deletes 4.1 kb, including both isoform 2b alternative exons.

Accession numbers: The GenBank accession numbers for sequences reported in this article are as follows: *odr-2* isoform 2b, AF324050; *odr-2* isoform 16, AF324051; *odr-2* isoform 18, AF324052; *hot-1*, AF324053; *hot-2*, AF324054; *hot3*, AF324055; *hot-4*, AF324056; *hot-5*, AF324057; *hot-6*, AF324058; *hot-7*, AF324059.

RESULTS

Chemotaxis to 2,3-pentanedione is mediated by AWC at low concentrations and by both AWA and AWC at high concentrations: *odr-2* mutants have strong defects in chemotaxis to benzaldehyde and isoamyl alcohol, two odors sensed by AWC, and moderate defects in chemotaxis to butanone, another AWC-sensed odorant (Bargmann *et al.* 1993). They respond normally to the AWA-sensed odorants diacetyl and pyrazine. In further characterization, we noted that *odr-2* mutants exhibited defective chemotaxis to low concentrations of the odorant 2,3-pentanedione (Figure 1B). The cells that detect 2,3-pentanedione have not been described, so we identified them by laser ablation in wild-type animals. Killing the two AWC neurons caused a striking defect in chemotaxis to 2,3-pentanedione (1:10,000 dilution), but killing the AWA neurons had no effect (Figure 1A). These results suggest that the AWC neurons sense 2,3-pentanedione and are consistent with the previous observation that *odr-2* affects only AWC responses.

At high concentrations of 2,3-pentanedione (1:10 dilution), *odr-2* mutants responded as well as wild type (Figure 1B). Similar residual responses to high concentrations of odorants have been observed in all olfactory mutants. For example, null mutants in the diacetyl receptor *odr-10* still respond to high concentrations of diacetyl (1:10 dilution; Sengupta *et al.* 1996) and *odr-2* mutants as well as null *odr-1* mutants still respond to high concentrations of benzaldehyde or isoamyl alcohol (Bargmann *et al.* 1993). These residual responses could reflect leakiness of the mutants, redundant olfactory mechanisms, or some kind of nonspecific odorant response.

We explored the high-concentration responses for two odorants, diacetyl and 2,3-pentanedione, because they exhibit responses over a broad range of odor concentrations and because they are structurally similar odorants that are recognized by different neurons (AWA and AWC, respectively). First, we killed either the AWA or the AWC neuron and tested responses to 1:10 dilutions of diacetyl or 2,3-pentanedione (Figure

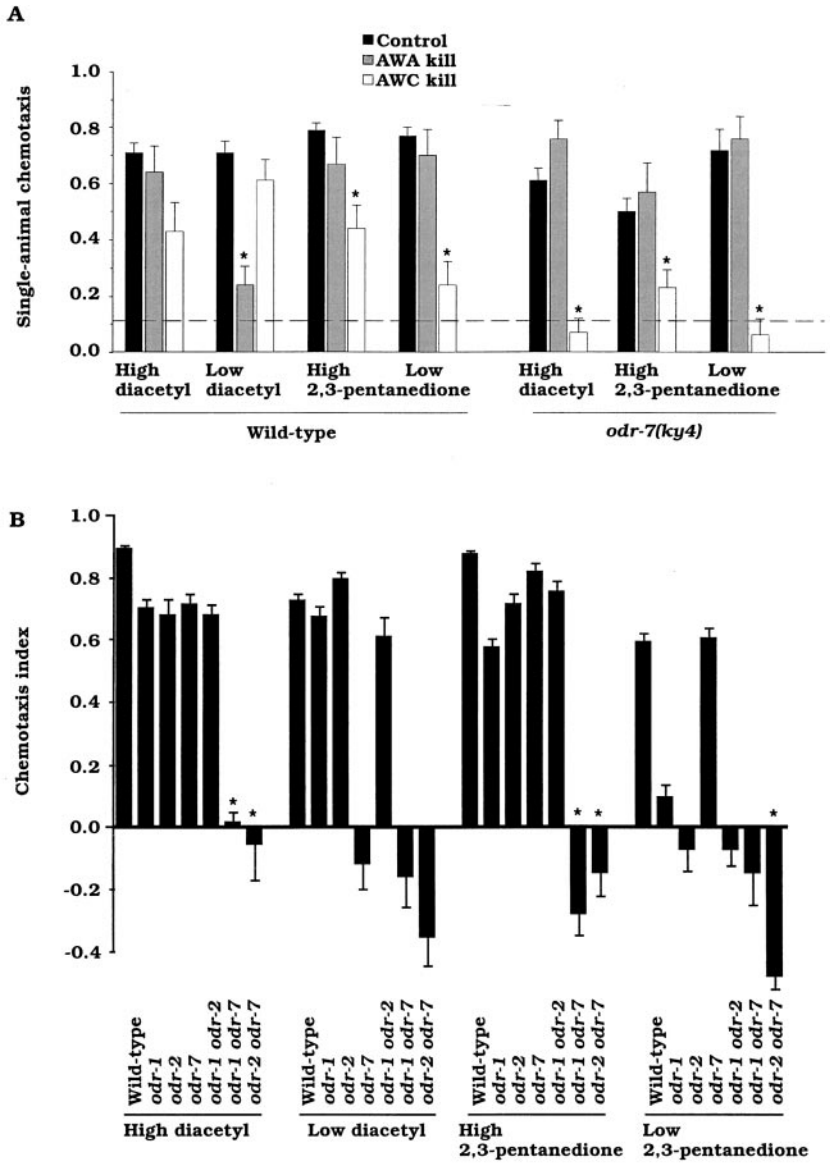

FIGURE 1.—(A) Single animal chemotaxis of control and laser-operated animals to diacetyl and 2,3-pentanedione. Chemotaxis index indicates the fraction of animals that gave a positive response in chemotaxis assays. This assay has a baseline false-positive rate of 0.11 in the absence of odorant, indicated by the dashed line. At least 16 assays were conducted for each data point. One data point (wild type, AWC kill, low diacetyl) was taken from BARGMANN *et al.* (1993). Error bars indicate the standard error of proportion. Odorant diluted in ethanol (1 μl) was used as an attractant. High concentrations were a 1:10 dilution; low concentrations were a 1:1000 dilution for diacetyl and a 1:10,000 dilution for 2,3-pentanedione. Asterisks denote values different from controls at $P < 0.01$. For the response to high diacetyl after AWC ablation, wild type differs from *odr-7* at $P < 0.01$. (B) Population chemotaxis assays of wild type, single, and double mutants to high and low odorant concentrations. 1.0, perfect chemotaxis; −1.0, perfect avoidance; 0.0, random responses to odorants. Mutants were *odr-1(n1936)*, *odr-2(n2145)*, and *odr-7(ky4)*. Values are the average of at least six independent assays per strain. Error bars indicate the standard error of the mean. Asterisks denote double mutants that are more defective than either single mutant at $P < 0.01$. Odorant dilutions were as in B, but there are differences in the scoring of population and single-animal assays, so the numbers in A and B cannot be compared directly.

1A; these dilutions are called "high diacetyl" and "high 2,3-pentanedione"). Chemotaxis to high diacetyl or high 2,3-pentanedione was not eliminated by killing the cell that sensed each odorant at low concentrations. Interestingly, killing AWC led to a slight defect in chemotaxis to both high diacetyl and high 2,3-pentanedione. This result suggests that AWC is more important at high diacetyl concentrations, whereas AWA is more important at low diacetyl concentrations.

To further explore the potential roles of AWA and AWC in the high-concentration responses, we took advantage of the *odr-7* mutant. *odr-7* encodes a transcription factor expressed only in AWA that is required for all known AWA functions (SENGUPTA *et al.* 1994). In *odr-7* mutants, AWA neurons are partially transformed toward an AWC fate based on expression of the AWC marker *str-2* (SAGASTI *et al.* 1999). When we repeated the AWA and AWC laser ablation experiments in an *odr-7* mutant background, we observed that the response to low concentrations of 2,3-pentanedione required AWC, as in wild-type animals (Figure 1A). Thus the partly transformed AWA neuron cannot mediate a response to 2,3-pentanedione. Interestingly, however, the responses to high diacetyl and high 2,3-pentanedione were dramatically reduced by killing AWC in the *odr-7* mutant background (Figure 1A). Killing the AWA neurons had no effect. This result suggests that the AWA and AWC neurons mediate redundant responses to high diacetyl and high 2,3-pentanedione: eliminating either AWA (with the specific *odr-7* mutation) or AWC (by cell killing) had little effect, but eliminating both AWA and AWC crippled the response.

If high concentrations of odors are sensed by both AWA and AWC, double mutants that eliminate the functions of both cells should exhibit defects that are not apparent in either single mutant. This model was tested

using well-characterized mutant strains. *odr-7* represents an ideal AWA mutant because of its specific cell fate defect. For AWC, there is no comparable cell fate mutant but a potential counterpart exists in *odr-1*, a guanylyl cyclase required for olfactory responses in AWC (L'Etoile and Bargmann 2000). Single mutants either in *odr-7* or in *odr-1* exhibited robust chemotaxis to high diacetyl and high 2,3-pentanedione (Figure 1B). *odr-1 odr-7* double mutants exhibited a dramatic defect in chemotaxis to high concentrations of odorants, as expected if both AWA and AWC are defective (Figure 1B). Indeed, 2,3-pentanedione actually became repulsive, perhaps because an underlying repulsion mediated by other cells was revealed when AWA and AWC functions were lost.

With this model in mind, double mutant analysis was used to further characterize the defects in *odr-2*. *odr-1 odr-2* double mutants exhibited defects that were comparable to either single mutant, sparing the response to high diacetyl and high pentanedione (Figure 1B). This result suggests that *odr-1* and *odr-2* affect the functions of the same cells, probably AWC, and that *odr-2* does not affect the AWA component of odor sensation. By contrast, *odr-2 odr-7* double mutants lost all responses to high diacetyl and high pentanedione. The simplest explanation for this result is that *odr-2* eliminates the AWC component of these responses, causing a synthetic phenotype when the AWA (*odr-7*) component is absent. We conclude that *odr-2* has profound effects on AWC function: it is required for the AWC component of chemotaxis to high or low 2,3-pentanedione, high diacetyl, benzaldehyde, and isoamyl alcohol.

Alternatively spliced *odr-2* mRNAs encode three predicted membrane-associated proteins with structural similarity to the Ly-6 superfamily: *odr-2* was previously localized between the endpoints of *nDf32* and *sDf30* on chromosome V (Bargmann *et al.* 1993). Its position was further refined and localized to the three overlapping cosmids NA2, VC5, and EB2. Each of these cosmids was capable of rescuing the benzaldehyde chemotaxis defect of *odr-2*(*n2145*) mutants (data not shown). A 13.4-kb *Kpn*I-*Spe*I subclone of EB2 rescued nearly as well as the complete cosmid, but further subcloning drastically curtailed rescue (Figure 2A).

The 7.6-kb *Kpn*I-*Stu*I fragment that showed partial rescue was used to screen a mixed-stage *C. elegans* cDNA library. A total of 12 cDNAs representing eight independent clones were isolated from 1.1×10^6 plaques. All cDNAs shared identical 3′ regions consisting of 453 nucleotides of open reading frame and 197 nucleotides of 3′ untranslated region (Figure 2, B–D). However, the 5′ ends appear to be alternatively spliced. Thus, these clones represent a family of transcripts predicted to encode three related but distinct protein products, which were called ODR-2 isoforms 2b, 16, and 18. ODR-2 2b possessed 250 nucleotides of divergent 5′ message spliced to the common region, with two potential in-frame start methionines, which would result in 40 or 50 isoform-specific amino termini residues (one clone). ODR-2 16 had 185 nucleotides of divergent 5′ sequence with a single in-frame start methionine resulting in 26 isoform-specific residues (one clone). ODR-2 18 had 131 (three clones) or 342 (one clone) nucleotides of divergent 5′ sequence with a single in-frame methionine resulting in 22 isoform-specific residues (four independent clones). The three shorter ODR-2 18 clones had 9, 7, and 1 nucleotides, respectively, of sequence matching the SL1 *trans*-spliced leader. Hemi-nested reverse-transcriptase (RT)-PCR of *C. elegans* mRNA using an SL1 primer and two *odr-2* common region primers confirmed that isoform 18 is *trans*-spliced and demonstrated that isoform 2b can also be SL1 *trans*-spliced 5 nucleotides upstream of the 5′ end of the original 2b cDNA isolate (data not shown). No additional *odr-2* isoforms were identified.

The four common exons shared by all ODR-2 isoforms are clustered in a 1.6-kb genomic region, while the three alternative N termini were located 9.0 kb (2b), 5.7 kb (16), and 3.3 kb (18) upstream of the common region (Figure 2B). Isoforms 16 and 18 are generated by a single alternative exon, whereas isoform 2b possesses two isoform-specific exons. Deletion of the common region from the 13.4-kb genomic fragment abolished *odr-2* rescuing activity, indicating that the cDNAs isolated represent *odr-2* (Figure 2A).

Each of the three alternative ODR-2 N termini contains a hydrophobic potential signal sequence (Figure 2, C and D). The extreme C terminus has a pronounced hydrophobic segment followed by a terminal arginine, consistent with a glycosylphosphatidylinositol membrane anchoring signal (Udenfriend and Kodukula 1995). The common region is relatively cysteine-rich, with 10 cysteines in the predicted mature protein. Its sequence suggests that ODR-2 might be membrane associated via a GPI anchor, with an extracellular domain containing disulfide linkages. BLAST searches of the GenBank database using predicted ODR-2 protein sequences did not identify significant homology to any previously characterized proteins.

Extracellular proteins often retain a characteristic cysteine spacing to maintain disulfide bridges required for proper protein structure. The abundance of cysteines in the ODR-2 common region invited comparison of the relative spacing of these residues with those in other proteins. ODR-2 shared a pattern of cysteine spacing with that found in the superfamily of Ly-6 domain-containing proteins (Table 1). The defining feature of these proteins is the presence of one or more domains of 10 cysteine residues with conserved spacing. Although very few noncysteine residues are conserved between the more divergent members of the Ly-6 superfamily, one of them, an asparagine immediately following the 10th cysteine, is also found in ODR-2 (Figure 2D). The spacing between some ODR-2 cysteines is in good agreement

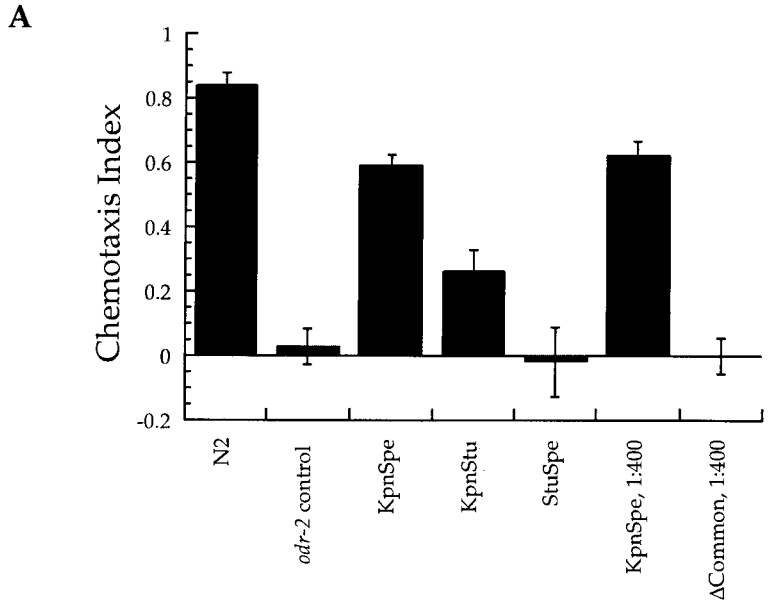
A
Chemotaxis Index
1
0.8
0.6
0.4
0.2
0
-0.2
N2
odr-2 control
KpnSpe
KpnStu
StuSpe
KpnSpe, 1:400
ΔCommon, 1:400

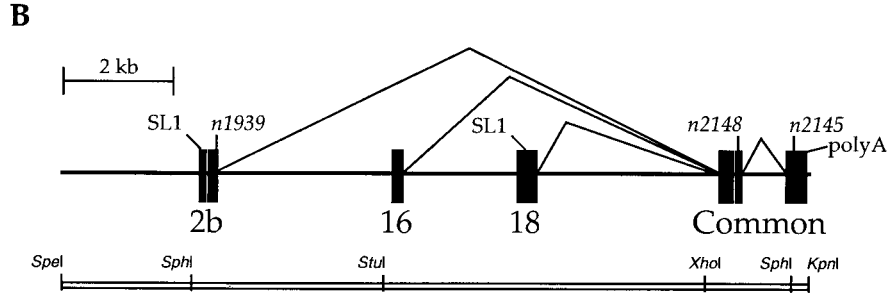
B
2 kb
SL1
n1939
SL1
n2148
n2145
polyA
2b
16
18
Common
SpeI
SphI
StuI
XhoI
SphI
KpnI

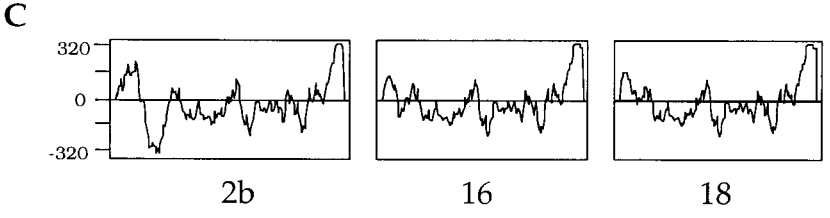
C
320
0
-320
2b
16
18

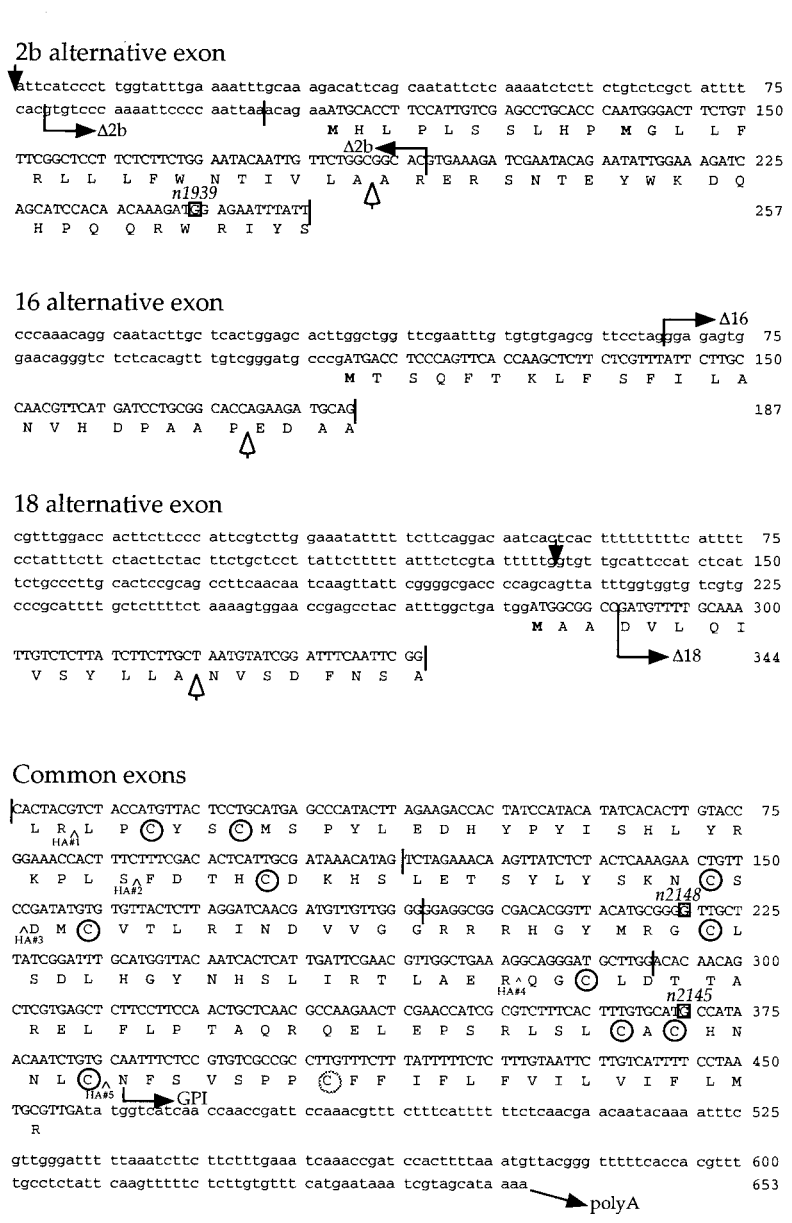
D
2b alternative exon
Δ2b
n1939
16 alternative exon
Δ16
18 alternative exon
Δ18
Common exons
n2148
n2145
GPI
polyA

TABLE 1

Cysteine spacing in the Ly-6 domain family members

	No. of residues between cysteines								
	1–2	2–3	3–4	4–5	5–6	6–7	7–8	8–9	9–10
	Ly-6 protein								
CD59 (human)	2	6	5	6	12	5	17	0	4
Ly-6A/F/G (mouse)	2	8	4	6	20	3	19	0	4
Lynx1 (mouse)	2	6	5	6	17	3	16	0	4
Sgp-2 (squid)	2	7	13	6	20	13	13	1	4
Drosophila	2	7	13	16	16	14	13	1	5
α-Cobratoxin	NA	NA	NA	5	20	3	10	0	4
ODR-2	2	25	14	3	20	20	25	1	4
HOT-1	2	25	14	3	20	24	23	1	4
HOT-2	2	25	13	3	21	24	25	1	4
HOT-3	2	26	13	3	22	22	21	1	4
HOT-4	ND	25	11	3	19	25	21	1	4
HOT-5	2	27	14	3	24	23	20	1	4
HOT-6	2	32	16	5	16	19	19	1	4
HOT-7	2	29	9	3	19	14	19	1	4

The 10 cysteines of the Ly-6 domain form disulfide bridges as follows: 1–5, 2–3, 4–6, 7–8, and 9–10. Snake venom long neurotoxins are unique in that they lack cysteines 2 and 3 and have an additional disulfide-linked cysteine pair between cysteines 5 and 6 that is not found in the rest of the Ly-6 domain superfamily (Ploug and Ellis 1994). Missing cysteine pairs result in some spacings being not applicable (NA). The complete sequence is not known for HOT-4, so the spacing between its first two cysteines is not determined (ND). Genes and their accession numbers are as follows: human CD59, JL0109; mouse Ly-6A.2, M73552; Ly-6F.1, X70922; Ly-6G.1, X70920; Lynx1, AF141377.1; Drosophila predicted protein, AAF53178.1. The sequences from Sgp-2 (Williams *et al.* 1988) and the long α-neurotoxin α-cobratoxin (Betzel *et al.* 1991) were determined from the listed sources. Coding regions of *hot* genes were not predicted by the *C. elegans* Genome Sequencing Consortium, with the exception of *hot-5* (K07A12.6), *hot-6* (C13G3.2), and *hot-7* (Y48B6A.9; our *hot-7* prediction was altered from the previously predicted gene in the last exon). For this analysis, potential coding sequences were predicted from F43D2 (*hot-1*), Y39B6.CTG10713 (*hot-2*), W02B8 (*hot-3*), and T12A2 (*hot-4*) (see Figure 6).

with those found in the Ly-6 superfamily, whereas others fall outside the previously observed range (Table 1). However, all of the cysteine spacings observed can be accommodated by the known structures of Ly-6 family genes, usually by increasing the loops formed between disulfide bridges (Figure 3A; Betzel *et al.* 1991; Fletcher *et al.* 1994; Kieffer *et al.* 1994).

To confirm the identity of *odr-2*, we characterized the mutations associated with the known *odr-2* alleles *n2145*, *n2148*, and *n1939* (Figure 2, B and D). All three mutations identified were G to A transitions, consistent with the properties of ethyl methanesulfonate mutagenesis. The *n2145* allele had a missense mutation in the common region converting the ninth cysteine to tyrosine,

Figure 2.—(A) Rescue of the *odr-2* benzaldehyde chemotaxis defect. Genomic subclones from the *odr-2* region were introduced into *odr-2(n2145)* animals and tested for ability to rescue benzaldehyde chemotaxis. *odr-2* expressing the *lin-15* co-injection marker alone was used as a negative control (*odr-2* control). All assays were done using a 1:600 dilution of benzaldehyde, except the last two columns (1:400 dilution). (B) Genomic organization of *odr-2*. The horizontal line represents the rescuing 13.4-kb *Kpn*I to *Spe*I genomic fragment (KpnSpe). Exons are represented by solid rectangles. The mutations found in the three alleles of *odr-2* and restriction sites used for generating deletion subclones in A are shown. SL1, site of addition of *trans*-splice leader. (C) Kyte-Doolittle hydrophobicity plots of the three predicted ODR-2 proteins. (D) *odr-2* sequence. (Top) Alternative isoforms were predicted from cDNA clones. Lowercase and uppercase nucleotides represent noncoding and coding regions, respectively. Vertical lines in the sequence represent the positions of introns. Solid arrowheads indicate sites where *trans*-splicing to SL1 leader RNA has been observed. Potential translation initiation methionines are in boldface. Open arrowheads indicate possible signal sequence cleavage sites (von Heijne 1986). In the 2b alternative exons, the G to A transition found in *n1939* is boxed; this results in a premature stop codon. The areas deleted in the Δ2b subclone, the Δ16 subclone, and the Δ18 subclone are indicated; the 3′ endpoints of the Δ16 subclone and the Δ18 subclone are in intron sequences. (Bottom) Sequence of the common region found in all *odr-2* cDNAs. G to A transitions found in *n2148* and *n2145* are boxed. Cysteine residues are circled. In Sgp-2, the glycosylphosphatidylinositol attachment occurs on the conserved asparagine immediately following the 10th cysteine, as indicated. Thus, the 11th cysteine of the common region may not be present in the mature forms of ODR-2. The locations of the five hemagglutinin (HA) epitope tag insertions are indicated. The coding region of *odr-2* partially overlaps the gene T01C4.2 predicted by the *C. elegans* Sequencing Consortium.

supporting an important structural role for the conserved cysteines in ODR-2. *n2148* had a missense mutation in the common region altering the glycine immediately before the sixth cysteine to aspartate. These mutations should affect all ODR-2 isoforms. *n1939* had a nonsense mutation in the 2b isoform alternative region, possibly implicating this isoform in chemotaxis.

ODR-2 is widely expressed in neurons, but apparently not in the AWC neurons: To determine where ODR-2 function might be required, a HA epitope tag was inserted in-frame into five different locations of the common region in an *odr-2* rescuing clone (Figure 2D). The five locations were chosen to minimize interference with the core regions of the Ly-6 domain on the basis of the known structure of CD59 (Figure 3A). Four of these five clones could fully rescue the isoamyl alcohol chemotaxis defect of *odr-2(n2145)* mutants; the fifth clone partly rescued the mutant (Figure 3B).

Whole-mount antibody staining of the transgenic animals with anti-HA antibodies revealed widespread expression that was restricted to neurons (Figure 4, A–C). Expression was observed at all larval stages and in the adult. Staining was concentrated in axonal processes, was less prominent in dendritic processes, and was excluded from the nucleus. Many classes of sensory neurons, interneurons, and motor neurons expressed ODR-2(HA). Because of the AWC chemosensory defects in *odr-2* mutant animals, it was significant that neither strong expression in AWC nor prominent staining in the amphid chemosensory cilia was observed. However, expression in the AWC axons would not have been distinguishable among the large bundle of axons in the nerve ring that express ODR-2 (Figure 4A). Indeed, few definitive cell identifications were possible because of the axonal localization of the protein.

To help identify the cells that express *odr-2*, genomic sequence upstream of each of the ODR-2 2b, 16, and 18 isoforms was used to direct expression of the GFP. Each of these three fusion genes generated distinct patterns of neuronal GFP expression (Figure 4, D–F). The expression patterns overlapped with the expression of the rescuing epitope-tagged ODR-2 protein, but probably did not represent all neurons that express the genomic clone. The regions upstream of each alternative start methionine interacted with other sequences to direct *odr-2*::GFP expression: a 10.8-kb *Sph*I fragment translational fusion that included both ODR-2 16 and 18 isoforms (Figure 2B) was expressed in neurons not seen in either ODR-2 16 or 18 GFP expression patterns (data not shown). Strong AWC expression was not observed in any of the GFP fusion genes. However, the ODR-2 2b promoter drove strong expression in two major targets of AWC, the AIB and AIZ interneurons (Figure 4D).

To explore the possibility that *odr-2* acts in AWC, the AWC-specific *str-2* promoter was used to drive expression of cDNAs representing all three isoforms of ODR-2.

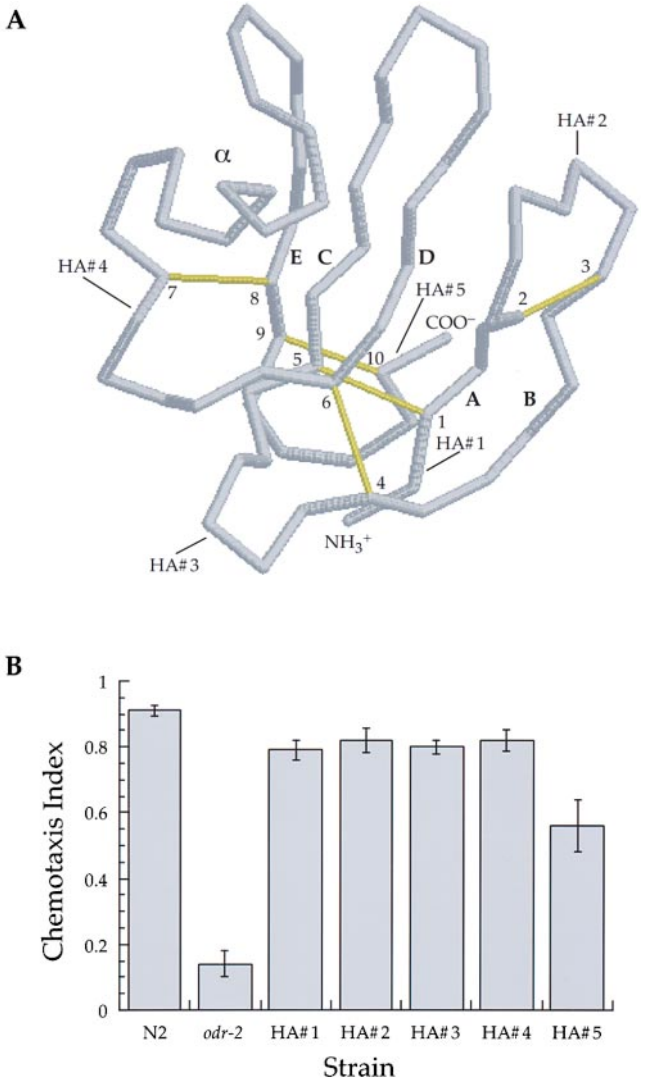

FIGURE 3.—(A) The solution structure of soluble CD59 (KIEFFER *et al.* 1994). The α-carbon backbone and disulfide bridges formed by the 10 cysteines, which are numbered consecutively, are shown. Strands A and B and strands C–E form two antiparallel β-sheets. The short α-helical segment that packs against one face of the C–E sheet is labeled. The predicted analogous regions of ODR-2 hemagglutinin epitope tag insertions are indicated. Coordinates of CD59 were obtained from the Brookhaven protein data bank, accession no. 1ERH. The structure was displayed using RasMac v2.5 by Roger Sayle, Biomolecular Structure, Glaxo Research and Development, Greenford, Middlesex, United Kingdom. (B) Epitope-tagged ODR-2 rescues the *odr-2* isoamyl alcohol chemotaxis defect. The HA epitope tag was introduced into the *odr-2* KpnSpe rescuing clone at five different locations in the common region. Each of these clones was tested for rescue of the *odr-2(n2145)* isoamyl alcohol chemotaxis defect.

These three clones were injected as a pool into *odr-2*(*n2145*) animals. No rescue of the isoamyl chemotaxis defect was observed (Figure 5A). In a second experiment, the *odr-3* promoter, which is expressed in AWC and a few other cells, was used to drive the ODR-2 2b isoform. This clone did not rescue the defects in the ODR-2

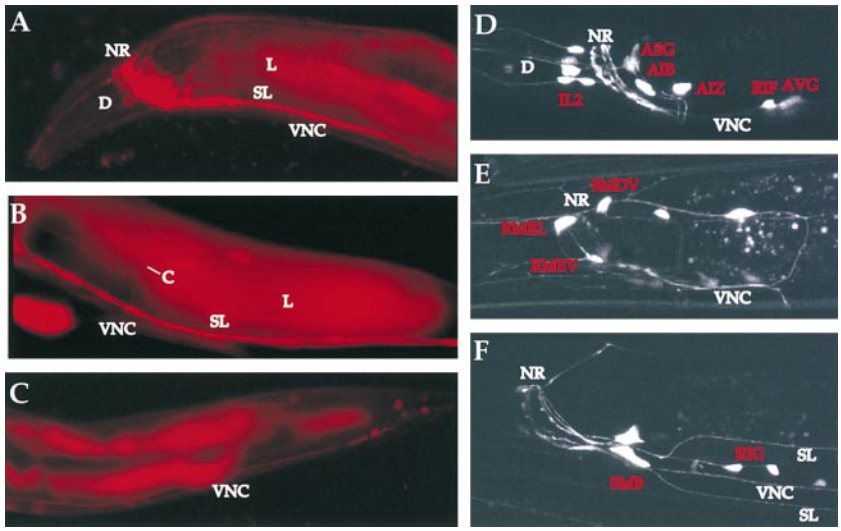

FIGURE 4.—(A–C) Expression of a rescuing epitope-tagged *odr-2* clone, HA#3, in the head, mid-body, and tail regions, respectively. The hemagglutinin epitope was introduced into the common region of ODR-2 and visualized by whole-mount antibody staining of adult animals. Anterior is to the left and dorsal is up. ODR-2 is expressed at high levels in axons and concentrated in the nerve ring (NR) and ventral nerve cord (VNC), although expression in other nerve bundles is also visible (L, lateral; SL, ventral sublateral; C, commissures). Only weak staining was observed in the region of sensory dendrites (D). Because ODR-2 is not present in the cell body in most cells, the neurons expressing these HA epitopes could not be identified. Expression is probably present in numerous classes of sensory neurons, interneurons, and motor neurons. Expression was not observed in AWC cell bodies. (D–F) Expression of *odr-2* GFP fusion clones. GFP expression patterns in the head/nerve ring region of adult animals were collected as confocal planes and projected onto the images shown; anterior is to the left and dorsal is up. Nonhead region neuronal GFP expression was also observed (data not shown). D–F show GFP driven by sequences upstream of the predicted translation start sites of *odr-2 (2b)*, *odr-2 (16)*, and *odr-2 (18)*, respectively. Expression driven by the 2b upstream region was observed in AIZ, AIB, AVG, RIF, PVP, and RIV interneurons, SIAV motor neurons, and IL2 and ASG sensory neurons. Faint expression driven by the 16 upstream region was observed in SMD and RME motor neurons, as well as in several other neurons in a variable pattern. Expression driven by the 18 upstream region was observed in SMB and RME motor neurons, in ALN and PLN sensory neurons, and in RIG interneurons. Neuron names are denoted in red and the names of nerve bundles are denoted in white (NR, nerve ring; VNC, ventral nerve cord; SL, ventral sublateral cords; D, dendrites).

2b-specific *odr-2(n1939)* mutant (data not shown). While these results suggest that AWC expression is not sufficient to rescue *odr-2*, they might have failed for other reasons such as poor cDNA expression.

ODR-2 isoforms can functionally substitute for one another: The identification of a nonsense mutation in *odr-2(n1939)* in the 2b isoform suggested that this isoform might be essential for ODR-2's role in chemotaxis. To test the requirement of each of the alternative ODR-2 isoforms in AWC-mediated chemotaxis, internal deletions in specific alternative isoforms were made in a rescuing subclone (Figure 5E). Surprisingly, deletions of the unique coding regions of the 2b, 16, and 18 isoforms individually (Δ2b or Δ16 or Δ18) or simultaneous deletion of the unique regions of the 2b and 16 isoforms (Δ2bΔ16) did not eliminate *odr-2* activity (Figure 5, B and C). However, simultaneous deletion of the unique regions for all three of the 2b, 16, and 18 isoforms (Δ2bΔ16Δ18) abolished chemotaxis rescue (Figure 5C). These results suggest that expression of at least one of the 2b, 16, or 18 isoforms is required for AWC-mediated chemotaxis and suggest that these isoforms can functionally substitute for one another. Unidentified isoforms may also contribute to ODR-2 function.

Additional deletions were generated to identify genomic regions necessary for *odr-2* rescue. A deletion that included 1.8 kb upstream of the ODR-2 18 isoform (Δ*Bst*EII) failed to rescue *odr-2*-mediated chemotaxis (Figure 5B). A deletion of 4.1 kb in the ODR-2 2b region (Δ*Cla*I) combined with the Δ16 deletion also abolished *odr-2* rescue (Figure 5B). These experiments identify potential regulatory regions in addition to the common coding exons that are required for *odr-2*-mediated chemotaxis.

To confirm that the *odr-2(n1939)* mutant phenotype resulted from the isoform 2b nonsense mutation, and not from an unidentified mutation in the common region, the mutation associated with *n1939* was introduced into a rescuing epitope-tagged clone. This nonsense mutation eliminated chemotaxis rescue of *odr-2* mutants (Figure 5D).

No anatomical defects are observed in *odr-2* (*n2145*) mutants: The enriched expression of functional epitope-tagged ODR-2 in axons suggested that it might play a role in axon outgrowth, guidance, or fasciculation. To visualize potential neuroanatomical defects, neuron-specific GFP reporters were each introduced into wild-type and *odr-2(n2145)* mutant animals. These GFP reporters were expressed in the AWC chemosensory neurons (STR-2:GFP; TROEMEL *et al.* 1999), AIY interneurons (TTX-3:GFP; HOBERT *et al.* 1997), and the neurons labeled by ODR-2 2b:GFP including interneurons AIB and AIZ. In all cases, the GFP expression and axon trajectories of the neurons were normal (data not shown). To attempt to detect more subtle defects in fasciculation, strains expressing GFP in multiple neurons were examined. No difference between wild-type and *odr-2* mutants was noted in strains expressing both

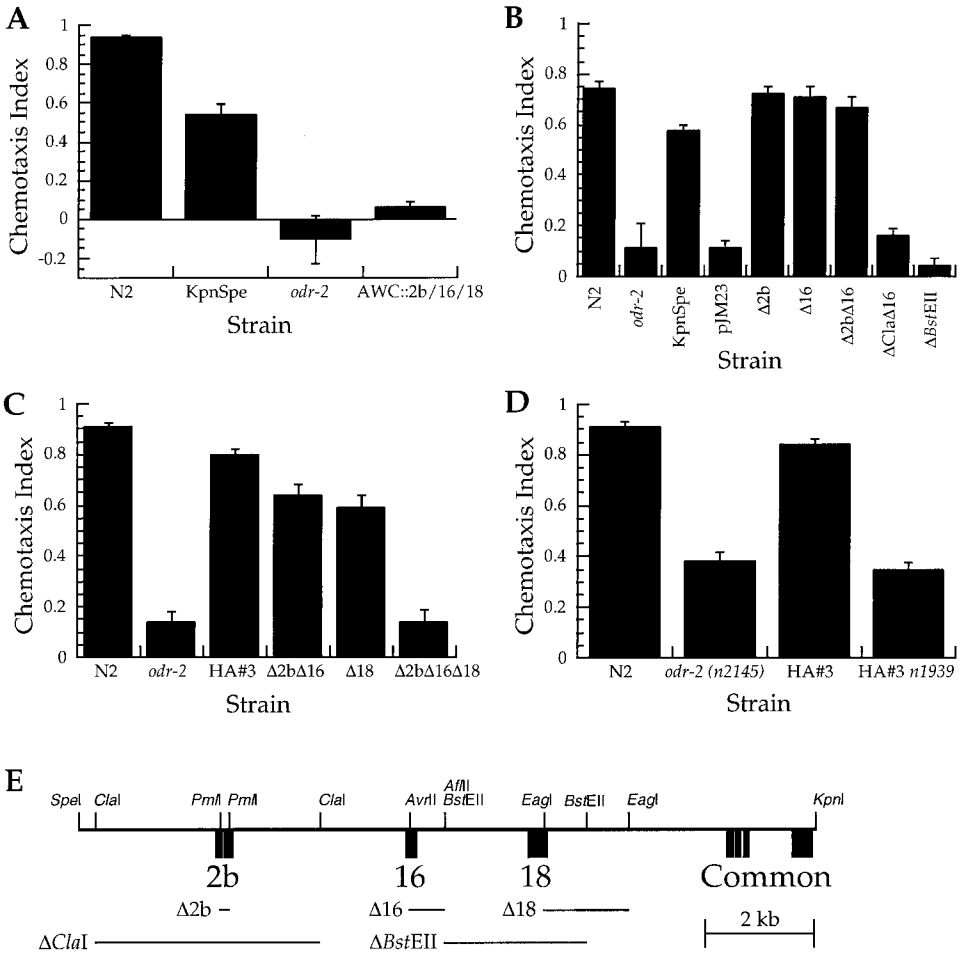

FIGURE 5.—(A) ODR-2 expressed in AWC may not rescue isoamyl alcohol chemotaxis. *odr-2* genomic and cDNA constructs were tested for ability to rescue chemotaxis to 1:100 isoamyl alcohol. Three subclones in which an AWC-specific promoter was used to drive *odr-2* 2b, 16, and 18 cDNA expression were pooled and injected into *odr-2(n2145)* animals. KpnSpe represents a rescuing 13.4-kb clone. Co-injection marker alone was used as a negative control (*odr-2*). (B) Coding and regulatory regions required for *odr-2* rescue. Deletions were made in the rescuing KpnSpe fragment that destroyed specific isoform coding regions or extended deletions previously shown not to affect *odr-2* chemotaxis rescue. These subclones were introduced into *odr-2(n2145)* animals and tested for chemotaxis to 1:800 benzaldehyde. N2 and *odr-2* are nontransgenic strains. Sequences defined by the ClaI and BstEII sites were required for rescue. Co-injection marker alone was used as an additional negative control (pJM23). (C) ODR-2 isoforms can functionally substitute for one another. Internal deletions that destroyed the alternative coding regions of *odr-2* were made in the rescuing epitope-tagged subclone, HA#3. Each of these clones was tested for rescue of the *odr-2(n2145)* isoamyl alcohol chemotaxis defect. The deletion clones ablated isoform 2b and 16 coding regions simultaneously (Δ2bΔ16), the 18 coding region individually (Δ18), and all three alternative isoform coding regions simultaneously (Δ2bΔ16Δ18). Only the triple deletion abrogated rescue. Expression of deleted clones was not characterized in detail. (D) The *n1939* mutation is sufficient to abolish *odr-2* function. The nonsense mutation in the isoform 2b alternative coding region was introduced into the rescuing epitope-tagged *odr-2* subclone, HA#3, and the resulting clone was tested for ability to rescue *odr-2(n2145)* chemotaxis to 1:100 isoamyl alcohol. Thus, in this context the ODR-2 2b coding region confers an essential function that is bypassed by deleting the 2b exon (B and C). (E) Genomic organization of *odr-2*. The horizontal line represents the rescuing 13.4-kb *Kpn*I to *Spe*I genomic fragment (KpnSpe). Exons are represented by solid rectangles. The shortened horizontal lines below the full-length KpnSpe fragment represent various internal deletions used in the experiments depicted in B and C. These deletions disrupt particular alternative isoforms (Δ2b, Δ16, and Δ18), or larger deletions (Δ*Bst*EII and Δ*Cla*I). The locations of restriction sites used for generating the subclones are shown.

STR-2:GFP and TTX-3:GFP (AWC and AIY) or in strains expressing both STR-2:GFP and ODR-2 2b:GFP (AWC and AIB/AIZ; data not shown).

The mammalian GPI-anchored protein Thy-1, has been detected in synaptic vesicles in addition to the plasma membrane (JENG *et al.* 1998). To examine the possibility that *odr-2* affected AWC synapses, a VAMP::GFP fusion protein that localizes to synaptic vesicles was expressed under an AWC-specific *str-2* promoter in wild-type and *odr-2* animals. No defects were apparent in *odr-2* mutants (G. CRUMP, personal communication). Localization of olfactory receptors to olfactory cilia was also normal in *odr-2* mutants, as was the structure of the cilia observed in electron micrographs (BARGMANN *et al.* 1993).

A family of *odr-2*-related genes in *C. elegans*: The rodent Ly-6 genes exist as a family of related genes. To determine whether *odr-2* might also belong to a multigene family, the sequenced regions of the *C. elegans* genome were analyzed by TBLASTN and PsiBLAST searches using ODR-2 sequence. Thus far, a total of seven paralogs of *odr-2* have been identified, and Ly-6-like coding regions analogous to the *odr-2* common region have been deduced (five are shown in Figure 6, Table 1). Notable features of these genes include conservation of all 10 cysteines and the spacing between them, the presence of an asparagine after the 10th cysteine, and a hydrophobic region at the extreme C terminus that is reminiscent of a GPI-anchorage signal (Figure 6). These homologs of *odr-2 (hot)* genes and *odr-2*

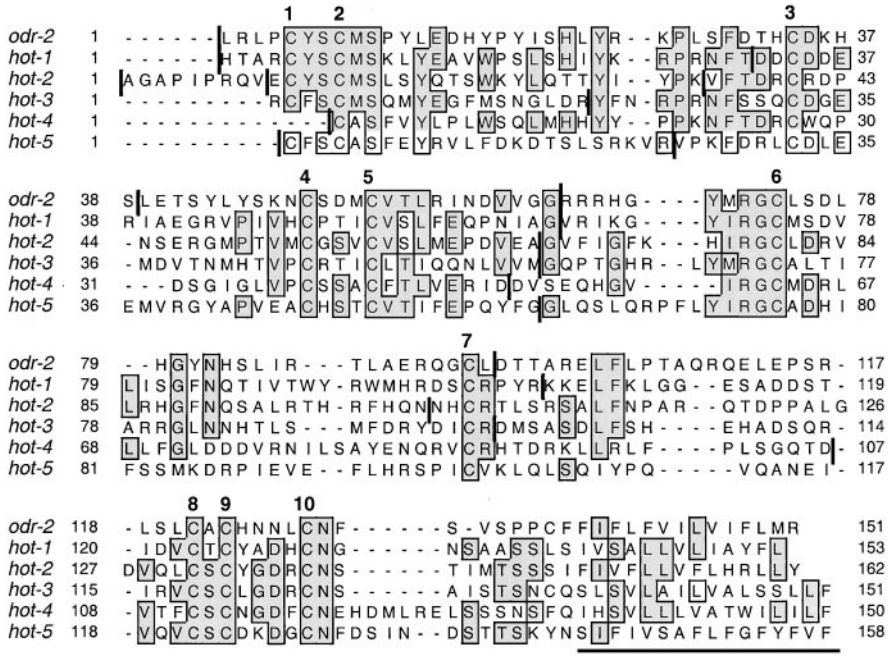

FIGURE 6.—Sequence alignment of the ODR-2 family of proteins. The 10 conserved cysteines are numbered. Locations of introns are noted by vertical lines. Residues identical in half or more of the family members are boxed and shaded. For *hot-1/2/4/5* there are no potential in-frame start methionines upstream of the listed coding regions, and probable upstream splice acceptor sites are noted. With *hot-2*, it is unclear which of the two possible splice sites upstream of the Ly-6 domain is used, so both are marked. Coding regions of *hot* genes were not predicted by the *C. elegans* Genome Sequencing Consortium, with the exception of *hot-5* (K07A12.6); potential coding sequences were predicted from genomic sequence of F43D2 (*hot-1*), Y39B6.CTG10713 *(hot-2)*, W02B8 *(hot-3)*, and T12A2 *(hot-4)*. Two other *hot*-like genes are more divergent from *odr-2* and *hot-1/2/3/4/5*, such that CLUSTALW alignment did not align the conserved cysteine residues; they are therefore not included in this alignment (*hot-6*, C13G3.2, and *hot-7*, a modified version of Y48B6A.9). Amino-terminal sequences of HOT-1A (MLLVDDHIIR NRRKIPDTPK RSYSNPYDTF VKLLIVVALA PKGVEASGER IYDETNYQGG NLPYK) and HOT-5A (MRQLPSILLI LVYFIRSVEL LK) have been determined from cDNAs. The horizontal line shows the hydrophobic residues at the C terminus.

have several conserved intron/exon boundaries, suggesting an evolutionary relationship with a common ancestral gene (Figure 6). Most of the paralogs lack in-frame codons for potential start methionines upstream of the Ly-6-like domain, but instead possess consensus splice acceptor sequences. Upstream exons that are spliced to the Ly-6 domain coding exons have been identified for *hot-1* and *hot-5* by RT-PCR and by a *C. elegans* expressed sequence tag (EST yk162), respectively. As in *odr-2*, the *hot-1a* and *hot-5a* 5′ exons are found far upstream of the Ly-6 domain coding region (6.5 kb and 2.6 kb upstream, respectively, data not shown). One interesting possibility is that the *hot* genes might be alternatively spliced to yield protein isoforms with alternative amino termini, like *odr-2. hot-1* may be expressed in neurons, since a GFP fusion gene with *hot-1* upstream sequence was expressed in a set of neurons that partially overlapped with the expression pattern of *odr-2* (data not shown).

DISCUSSION

odr-2 mutants exhibit impaired chemotaxis to volatile attractants sensed by the AWC olfactory neurons. As has been observed in other olfactory mutants, *odr-2* chemotaxis defects are observed in a limited range of odor concentrations. We considered three potential explanations for this result: the mutations could be leaky, so that some gene function is always retained; the olfactory neurons could become less tuned to specific odors at high odor concentrations, leading to redundancy between olfactory neurons; and there could be nonolfactory or nonneuronal mechanisms for detecting high odorant concentrations. By killing neurons in wild-type and mutant animals, we found that the AWA and AWC olfactory neurons sense a wider range of odors at high concentrations than at low concentrations. Moreover, double mutants that eliminated both AWA and AWC exhibit a dramatic synthetic defect in responses to high odor concentrations. These results favor the model that cellular redundancy between olfactory neurons is present at high odorant concentrations. This loss of specificity is analogous to observations in the mammalian olfactory system, where increasing odor concentrations activate an increasingly large number of olfactory neurons (MALNIC *et al.* 1999). By contrast, in the pheromone-sensing vomeronasal system of the rodent, neurons are highly selective for a single pheromone across a range of concentrations (LEINDERS-ZUFALL *et al.* 2000).

odr-2 encodes a novel protein with at least three isoforms generated by alternative splicing. Sequence analysis suggests that ODR-2 is an extracellular or membrane-associated protein, and the presence of a hydrophobic sequence at its extreme C terminus suggests that it could be anchored to the plasma membrane by a GPI linkage. Spacing between 10 cysteine residues in the ODR-2 common region resembles the spacing in a domain found in the Ly-6 superfamily of proteins, which are commonly GPI-linked (GUMLEY *et al.* 1995). Ly-6 proteins share sequence similarity in a domain of ~75 amino acids, defined by the conservation of 10 cysteine residues with a characteristic spacing pattern (LECLAIR *et al.* 1986;

van de Rijn *et al.* 1989; Friedman *et al.* 1990; Roldan *et al.* 1990; Betzel *et al.* 1991; Davies and Lachmann 1993; Fletcher *et al.* 1994; Kieffer *et al.* 1994; Ohkura *et al.* 1994; Ploug and Ellis 1994; Brakenhoff *et al.* 1995; Palfree 1996; Miwa *et al.* 1999). ODR-2 might be a distant relative of these proteins that shares their structure.

Deleting each of the three alternative first coding exons of *odr-2* individually does not affect the ability of the *odr-2* clone to rescue chemotaxis. Paradoxically, a premature stop codon within the ODR-2 2b isoform in the *odr-2(n1939)* allele abolishes ODR-2 function. Deletion of the ODR-2 2b-specific exons might alter splicing or interactions between the alternative promoters and enhancer sequences, allowing expression of the ODR-2 16 or 18 isoform in the cells that previously expressed only the ODR-2 2b isoform.

An HA-tagged ODR-2 protein in a rescuing genomic clone is expressed exclusively in neurons, including sensory, motor, and interneurons, and is concentrated in the axons. However, we could not easily detect *odr-2* expression in AWC, and directed expression of *odr-2* in AWC did not rescue its olfactory defect. Since the directed expression experiments were done with *odr-2* cDNAs, the negative results could reflect a problem with specific isoforms or cDNA expression levels. With these limitations, we suggest that ODR-2 might act in another neuron that modulates AWC function in chemotaxis, or it might be required in AWC at a specific time in development.

The AWC neurons appear normal in *odr-2* mutants by a variety of criteria. They express the AWC-specific gene *str-2*, they have morphologically normal cilia and axons, and the AWC axons fasciculate with the AIY axon, the major target of AWC (White *et al.* 1986). The axons of AIY and two other potential AWC targets, AIB and AIZ, are also apparently normal. Thus *odr-2* is not required for the development of any of the neurons that are known to be essential for AWC chemotaxis. We speculate that *odr-2* may play a modulatory role in neurons that regulate AWC or downstream interneurons.

odr-2 has a surprisingly specific mutant phenotype considering its widespread neuronal expression. AWC-mediated chemotaxis is disrupted, but chemotaxis mediated by AWA (odorants) or ASE (water-soluble attractants) is spared, and responses to ASH repellents and the dauer pheromone are also normal (Bargmann *et al.* 1993; data not shown). Locomotion is apparently normal, despite *odr-2* expression in many motor neurons and interneurons. *odr-2* might have a function that is regulatory rather than essential in the neurons that express it, or functional overlap between *odr-2* and the related *hot* genes may mask other effects. However, none of the three *odr-2* mutations are definitive null alleles, so a more severe phenotype could result from the complete absence of *odr-2* function.

The Ly-6 domain protein lynx1 has recently been shown to modulate the activity of nicotinic acetylcholine receptors, a function analogous to the function of the related snake venom neurotoxins (Betzel *et al.* 1991; Miwa *et al.* 1999). lynx1 and the snake neurotoxins are equally different from each other and from ODR-2 by sequence. The HA-tagged ODR-2 clone is expressed in cholinergic motor neurons and in neurons that synapse onto cholinergic motor neurons, consistent with a possible role for ODR-2 in modifying cholinergic transmission. However, many other models are possible: for example, ODR-2 proteins might act as cell surface markers that allow neurons to recognize each other during fasciculation or synaptic maintenance, or ODR-2 could modulate neuronal function as part of a different neurotransmitter receptor signaling pathway. Ly-6 domain proteins have been proposed to have many different functions in cell signaling and cell adhesion. Family members include the rodent Ly-6 cell surface markers (LeClair *et al.* 1986; Palfree *et al.* 1988; Friedman *et al.* 1990; Palfree 1996), human complement-mediated lysis inhibitor CD59 (Davies and Lachmann 1993), the neuronal protein lynx1 (Miwa *et al.* 1999), keratinocyte adhesion molecule E48 (Brakenhoff *et al.* 1995), human GPI-linked urokinase plasminogen activator receptor (Roldan *et al.* 1990; Ploug and Ellis 1994), both subunits of the snake phospholipase A_2 inhibitor (PLA2-I; Ohkura *et al.* 1994), and a number of snake neurotoxins (Betzel *et al.* 1991). In addition, the extracellular domain of the TGFβ type I receptor kinase contains a Ly-6-like repeat (Jokiranta *et al.* 1995), as does its *C. elegans* homolog, *daf-1* (Georgi *et al.* 1990). Ly-6 members have been implicated in modulation of extracellular matrix interactions (Wei *et al.* 1996), cell adhesion (Bamezai and Rock 1995; Brakenhoff *et al.* 1995), signal transduction (Jokiranta *et al.* 1995), regulation of plasminogen activation (Plesner *et al.* 1997), and protection against complement-mediated lysis (Davies and Lachmann 1993). A mouse mutation in one Ly-6 protein causes subtle defects in T-cell activation (Stanford *et al.* 1997).

ODR-2 and the related HOT proteins might be part of a larger signaling complex on neurons. The growth factors glial cell line-derived neurotrophic factor and neurturin are recognized by GPI-linked proteins that signal by activating a shared transmembrane tyrosine kinase subunit (Durbec *et al.* 1996; Jing *et al.* 1996, 1997; Treanor *et al.* 1996; Trupp *et al.* 1996; Baloh *et al.* 1997; Buj-Bello *et al.* 1997; Klein *et al.* 1997). Similarly, the GPI-linked ciliary neurotrophic factor receptor α-subunit interacts with transmembrane proteins to signal to cells (Davis *et al.* 1993; Stahl and Yancopoulos 1994).

Previous studies of olfactory signaling in *C. elegans* have identified G protein-coupled receptors and signaling pathways that might be directly involved in the perception of odorants, as well as genes involved in olfactory neuron development. *odr-2* disrupts olfaction without

causing overt developmental defects in the AWC olfactory neurons, and ODR-2 protein seems to be in axons and not in sensory cilia. These findings suggest that unlike the previously identified molecules, ODR-2 may act downstream of chemosensory signaling, either at olfactory synapses or outside the chemosensory neurons. Further characterization of *odr-2* may lead to a better understanding of the neural circuit that mediates chemosensory behaviors.

We thank Kate Wesseling, Penny Mapa, Liqin Tong, Shannon Grantner, and Yongmei Zhang for expert sequencing assistance; Tim Yu for generating the GFP confocal images; Alan Coulson and John Sulston for supplying cosmids; Y. Kohara for providing EST sequence; Bob Barstead for the cDNA library; Gary Ruvkun for *ttx-3*::GFP; and the *C. elegans* Sequencing Consortium for providing an invaluable resource to the research community. P.S. was supported by the American Cancer Society, California Division. J.H.C. was supported by the UCSF Medical Scientist Training Program. C.I.B. is an Investigator of the Howard Hughes Medical Institute. This work was supported by grants from the National Institutes of Health, National Institute on Deafness and Other Communication Disorders.

LITERATURE CITED

Altschul, S. F., W. Gish, W. Miller, E. W. Myers and D. J. Lipman, 1990 Basic local alignment search tool. J. Mol. Biol. **215:** 403–410.

Baloh, R. H., M. G. Tansey, J. P. Golden, D. J. Creedon, R. O. Heuckeroth *et al.*, 1997 TrnR2, a novel receptor that mediates neurturin and GDNF signaling through Ret. Neuron **18:** 793–802.

Bamezai, A., and K. L. Rock, 1995 Overexpressed Ly-6A.2 mediates cell-cell adhesion by binding a ligand expressed on lymphoid cells. Proc. Natl. Acad. Sci. USA **92:** 4294–4298.

Bargmann, C. I., 1993 Genetic and cellular analysis of behavior in *C. elegans*. Annu. Rev. Neurosci. **16:** 47–71.

Bargmann, C. I., and L. Avery, 1995 Laser killing of cells in *Caenorhabditis elegans*. Methods Cell Biol. **48:** 225–250.

Bargmann, C. I., E. Hartwieg and H. R. Horvitz, 1993 Odorant-selective genes and neurons mediate olfaction in *C. elegans*. Cell **74:** 515–527.

Betzel, C., G. Lange, G. P. Pal, K. S. Wilson, A. Maelicke *et al.*, 1991 The refined crystal structure of alpha-cobratoxin from Naja naja siamensis at 2.4-A resolution. J. Biol. Chem. **266:** 21530–21536.

Brakenhoff, R. H., M. Gerretsen, E. M. Knippels, M. van Dijk, H. van Essen *et al.*, 1995 The human E48 antigen, highly homologous to the murine Ly-6 antigen ThB, is a GPI-anchored molecule apparently involved in keratinocyte cell-cell adhesion. J. Cell Biol. **129:** 1677–1689.

Brenner, S., 1974 The genetics of *Caenorhabditis elegans*. Genetics **77:** 71–94.

Buj-Bello, A., J. Adu, L. G. Pinon, A. Horton, J. Thompson *et al.*, 1997 Neurturin responsiveness requires a GPI-linked receptor and the Ret receptor tyrosine kinase. Nature **387:** 721–724.

C. elegans Sequencing Consortium, 1998 Genome sequence of the nematode *C. elegans*: a platform for investigating biology. Science **282:** 2012–2018.

Coburn, C. M., and C. I. Bargmann, 1996 A putative cyclic nucleotide-gated channel is required for sensory development and function in *C. elegans*. Neuron **17:** 695–706.

Colbert, H. A., T. L. Smith and C. I. Bargmann, 1997 OSM-9, a novel protein with structural similarity to channels, is required for olfaction, mechanosensation, and olfactory adaptation in *Caenorhabditis elegans*. J. Neurosci. **17:** 8259–8269.

Davies, A., and P. J. Lachmann, 1993 Membrane defence against complement lysis: the structure and biological properties of CD59. Immunol. Res. **12:** 258–275.

Davis, S., T. H. Aldrich, N. Stahl, L. Pan, T. Taga *et al.*, 1993 LIFR beta and gp130 as heterodimerizing signal transducers of the tripartite CNTF receptor. Science **260:** 1805–1808.

Durbec, P., C. V. Marcos-Gutierrez, C. Kilkenny, M. Grigoriou, K. Wartiowaara *et al.*, 1996 GDNF signalling through the Ret receptor tyrosine kinase. Nature **381:** 789–793.

Dwyer, N. D., E. R. Troemel, P. Sengupta and C. I. Bargmann, 1998 Odorant receptor localization to olfactory cilia is mediated by ODR-4, a novel membrane-associated protein. Cell **93:** 455–466.

Fire, A., S. W. Harrison and D. Dixon, 1990 A modular set of lacZ fusion vectors for studying gene expression in *Caenorhabditis elegans*. Gene **93:** 189–198.

Fletcher, C. M., R. A. Harrison, P. J. Lachmann and D. Neuhaus, 1994 Structure of a soluble, glycosylated form of the human complement regulatory protein CD59. Structure **2:** 185–199.

Friedman, S., R. G. Palfree, S. Sirlin and U. Hammerling, 1990 Analysis of three distinct Ly6-A-related cDNA sequences isolated from rat kidney. Immunogenetics **31:** 104–111.

Georgi, L. L., P. S. Albert and D. L. Riddle, 1990 *daf-1*, a *C. elegans* gene controlling dauer larva development, encodes a novel receptor protein kinase. Cell **61:** 635–645.

Gumley, T. P., I. F. McKenzie and M. S. Sandrin, 1995 Tissue expression, structure and function of the murine Ly-6 family of molecules. Immunol. Cell Biol. **73:** 277–296.

Hobert, O., I. Mori, Y. Yamashita, H. Honda, Y. Ohshima *et al.*, 1997 Regulation of interneuron function in the *C. elegans* thermoregulatory pathway by the ttx-3 LIM homeobox gene. Neuron **19:** 345–357.

Jeng, C. J., S. A. McCarroll, T. F. Martin, E. Floor, J. Adams *et al.*, 1998 Thy-1 is a component common to multiple populations of synaptic vesicles. J. Cell Biol. **140:** 685–698.

Jing, S., D. Wen, Y. Yu, P. L. Holst, Y. Luo *et al.*, 1996 GDNF-induced activation of the ret protein tyrosine kinase is mediated by GDNFR-alpha, a novel receptor for GDNF. Cell **85:** 1113–1124.

Jing, S., Y. Yu, M. Fang, Z. Hu, P. L. Holst *et al.*, 1997 GFRalpha-2 and GFRalpha-3 are two new receptors for ligands of the GDNF family. J. Biol. Chem. **272:** 33111–33117.

Jokiranta, T. S., J. Tissari, O. Teleman and S. Meri, 1995 Extracellular domain of type I receptor for transforming growth factor-beta: molecular modelling using protectin (CD59) as a template. FEBS Lett. **376:** 31–36.

Kieffer, B., P. C. Driscoll, I. D. Campbell, A. C. Willis, P. A. van der Merwe *et al.*, 1994 Three-dimensional solution structure of the extracellular region of the complement regulatory protein CD59, a new cell-surface protein domain related to snake venom neurotoxins. Biochemistry **33:** 4471–4482.

Klein, R. D., D. Sherman, W. H. Ho, D. Stone, G. L. Bennett *et al.*, 1997 A GPI-linked protein that interacts with Ret to form a candidate neurturin receptor. Nature **387:** 717–721.

Komatsu, H., I. Mori, J. S. Rhee, N. Akaike and Y. Ohshima, 1996 Mutations in a cyclic nucleotide-gated channel lead to abnormal thermosensation and chemosensation in *C. elegans*. Neuron **17:** 707–718.

LeClair, K. P., R. G. Palfree, P. M. Flood, U. Hammerling and A. Bothwell, 1986 Isolation of a murine Ly-6 cDNA reveals a new multigene family. EMBO J. **5:** 3227–3234.

Leinders-Zufall, T., A. P. Lane, A. C. Puche, W. Ma, M. V. Novotny *et al.*, 2000 Ultrasensitive pheromone detection by mammalian vomeronasal neurons. Nature **405:** 792–796.

L'Etoile, N. D., and C. I. Bargmann, 2000 Olfaction and odor discrimination are mediated by the *C. elegans* guanylyl cyclase ODR-1. Neuron **25:** 575–586.

Low, M. G., 1989 The glycosyl-phosphatidylinositol anchor of membrane proteins. Biochim. Biophys. Acta **988:** 427–454.

Malnic, B., J. Hirono, T. Sato and L. B. Buck, 1999 Combinatorial receptor codes for odors. Cell **96:** 713–723.

Mello, C. C., J. M. Kramer, D. Stinchcomb and V. Ambros, 1991 Efficient gene transfer in *C.elegans*: extrachromosomal maintenance and integration of transforming sequences. EMBO J. **10:** 3959–3970.

Miwa, J. M., I. Ibanez-Tallon, G. W. Crabtree, R. Sanchez, A. Sali *et al.*, 1999 lynx1, an endogenous toxin-like modulator of nicotinic acetylcholine receptors in the mammalian CNS. Neuron **23:** 105–114.

Ohkura, N., S. Inoue, K. Ikeda and K. Hayashi, 1994 The two subunits of a phospholipase A2 inhibitor from the plasma of

Thailand cobra having structural similarity to urokinase-type plasminogen activator receptor and LY-6 related proteins. Biochem. Biophys. Res. Commun. **204:** 1212–1218.

Palfree, R. G., 1996 Ly-6-domain proteins—new insights and new members: a C-terminal Ly-6 domain in sperm acrosomal protein SP-10. Tissue Antigens **48:** 71–79.

Palfree, R. G., S. Sirlin, F. J. Dumont and U. Hammerling, 1988 N-terminal and cDNA characterization of murine lymphocyte antigen Ly-6C.2. J. Immunol. **140:** 305–310.

Plesner, T., N. Behrendt and M. Ploug, 1997 Structure, function and expression on blood and bone marrow cells of the urokinase-type plasminogen activator receptor, uPAR. Stem Cells **15:** 398–408.

Ploug, M., and V. Ellis, 1994 Structure-function relationships in the receptor for urokinase-type plasminogen activator. Comparison to other members of the Ly-6 family and snake venom alpha-neurotoxins. FEBS Lett. **349:** 163–168.

Roayaie, K., J. G. Crump, A. Sagasti and C. I. Bargmann, 1998 The G alpha protein ODR-3 mediates olfactory and nociceptive function and controls cilium morphogenesis in *C. elegans* olfactory neurons. Neuron **20:** 55–67.

Roldan, A. L., M. V. Cubellis, M. T. Masucci, N. Behrendt, L. R. Lund *et al.*, 1990 Cloning and expression of the receptor for human urokinase plasminogen activator, a central molecule in cell surface, plasmin dependent proteolysis. EMBO J. **9:** 467–474. (erratum: EMBO J. **9:** 1674).

Sagasti, A., O. Hobert, E. R. Troemel, G. Ruvkun and C. I. Bargmann, 1999 Alternative olfactory neuron fates are specified by the LIM homeobox gene lim-4. Genes Dev. **13:** 1794–1806.

Sambrook, J., E. F. Fritsch and T. Maniatis, 1989 *Molecular Cloning: A Laboratory Manual.* Cold Spring Harbor Laboratory Press, Cold Spring Harbor, NY.

Sengupta, P., H. A. Colbert and C. I. Bargmann, 1994 The *C. elegans* gene *odr-7* encodes an olfactory-specific member of the nuclear receptor superfamily. Cell **79:** 971–980.

Sengupta, P., J. H. Chou and C. I. Bargmann, 1996 *odr-10* encodes a seven transmembrane domain olfactory receptor required for responses to the odorant diacetyl. Cell **84:** 899–909.

Stahl, N., and G. D. Yancopoulos, 1994 The tripartite CNTF receptor complex: activation and signaling involves components shared with other cytokines. J. Neurobiol. **25:** 1454–1466.

Stanford, W. L., S. Haque, R. Alexander, X. Liu, A. M. Latour *et al.*, 1997 Altered proliferative response by T lymphocytes of Ly-6A (Sca-1) null mice. J. Exp. Med. **186:** 705–717.

Su, B., G. L. Waneck, R. A. Flavell and A. L. Bothwell, 1991 The glycosyl phosphatidylinositol anchor is critical for Ly-6A/E-mediated T cell activation. J. Cell Biol. **112:** 377–384.

Sulston, J., Z. Du, K. Thomas, R. Wilson, L. Hillier *et al.*, 1992 The *C. elegans* genome sequencing project: a beginning. Nature **356:** 37–41.

Thompson, J. D., D. G. Higgins and T. J. Gibson, 1994 CLUSTAL W: improving the sensitivity of progressive multiple sequence alignment through sequence weighting, position-specific gap penalties and weight matrix choice. Nucleic Acids Res. **22:** 4673–4680.

Treanor, J. J., L. Goodman, F. de Sauvage, D. M. Stone, K. T. Poulsen *et al.*, 1996 Characterization of a multicomponent receptor for GDNF. Nature **382:** 80–83.

Troemel, E. R., A. Sagasti and C. I. Bargmann, 1999 Lateral signaling mediated by axon contact and calcium entry regulates asymmetric odorant receptor expression in *C. elegans.* Cell **99:** 387–398.

Trupp, M., E. Arenas, M. Fainzilber, A. S. Nilsson, B. A. Sieber *et al.*, 1996 Functional receptor for GDNF encoded by the c-ret proto-oncogene. Nature **381:** 785–788.

Udenfriend, S., and K. Kodukula, 1995 How glycosylphosphatidylinositol-anchored membrane proteins are made. Annu. Rev. Biochem. **64:** 563–591.

van de Rijn, M., S. Heimfeld, G. J. Spangrude and I. L. Weissman, 1989 Mouse hematopoietic stem-cell antigen Sca-1 is a member of the Ly-6 antigen family. Proc. Natl. Acad. Sci. USA **86:** 4634–4638.

von Heijne, G., 1986 A new method for predicting signal sequence cleavage sites. Nucleic Acids Res. **14:** 4683–4690.

Wei, Y., M. Lukashev, D. I. Simon, S. C. Bodary, S. Rosenberg *et al.*, 1996 Regulation of integrin function by the urokinase receptor. Science **273:** 1551–1555.

White, J. G., E. Southgate, J. N. Thomson and S. Brenner, 1986 The structure of the nervous system of the nematode *Caenorhabditis elegans.* Philos. Trans. R. Soc. Lond. B Biol. Sci. **314:** 1–340.

Williams, A. F., A. G. Tse and J. Gagnon, 1988 Squid glycoproteins with structural similarities to Thy-1 and Ly-6 antigens. Immunogenetics **27:** 265–272.

Communicating editor: R. K. Herman